Influence of Conductance Changes on Patch Clamp Capacitance Measurements Using a Lock-In Amplifier and Limitations of the Phase Tracking Technique

Knut Debus, Jana Hartmann, Gordan Kilic, and Manfred Lindau
Abteilung Molekulare Zellforschung, Max-Planck-Institut für Medizinische Forschung, Jahnstrasse 29, 69120 Heidelberg, Germany

ABSTRACT We characterized the influence of conductance changes on whole-cell patch clamp capacitance measurements with a lock-in amplifier and the limitations of the phase-tracking method by numerical computer simulations, error formulas, and experimental tests. At correct phase setting, the artifacts in the capacitance measurement due to activation of linear conductances are small. The cross talk into the capacitance trace is well approximated by the second-order term in the Taylor expansion of the admittance. In the case of nonlinear current-voltage relationships, the measured conductance corresponds to the slope conductance in the range of the sine wave amplitude, and the cross talk into the capacitance trace corresponds to the second-order effect of the slope conductance. The finite gating kinetics of voltage-dependent channels generate phase-shifted currents. These lead to major artifacts in the capacitance measurements when the angular frequency of the sine wave is close to the kinetic rate constant of the channel. However, when the channel kinetics are sufficiently slow, or sufficiently fast, the cross talk is still close to the second-order effect of the measured conductance. The effects of activation of voltage-dependent currents on the capacitance measurements may be estimated, provided a detailed characterization of the kinetics and voltage dependence is available. A phase error of the lock-in amplifier of a few degrees leads to significant projections. The phase-tracking method can be used to keep the phase aligned only during periods of low membrane conductance. However, nonideal properties of the equivalent circuit, in particular the fast capacitance between the pipette and the bath solutions, may lead to large phase errors when the phase-tracking method is used, depending on the electrical properties of the cell. In this article we provide practical values, setting the range where possible artifacts are below defined limits. For proper evaluation of capacitance measurements, the capacitance and conductance traces should always be displayed together.

INTRODUCTION

Time-resolved patch clamp capacitance measurements are now widely used to study the changes in plasma membrane area associated with exocytosis and endocytosis (Lindau, 1991). For high resolution recordings, a sinusoidal voltage is added to the holding potential, and the resulting current is analyzed by a two-phase lock-in amplifier. When the phase of the lock-in amplifier is properly adjusted, the two outputs directly provide the changes of membrane conductance in one channel and the changes of membrane capacitance in the other channel (Neher and Marty, 1982; Joshi and Fernandez, 1988; Lindau and Neher, 1988; Gillis, 1995); this method is widely used to detect very small capacitance changes and the opening of individual fusion pores in single secretory granules (Breckenridge and Almers, 1987; Spruce et al., 1990; Lindau, 1991; Hartmann and Lindau, 1995). This is possible when the passive electrical properties of the whole-cell configuration can be represented by membrane conductance and capacitance in series with the pipette resistance.

Neurons, nerve terminals, electrically excitable endocrine cells, and many other exocytotic cells contain various types of voltage-dependent channels, which cannot be accounted for by a simple RC-equivalent circuit (Hodgkin and Huxley, 1952; Cole, 1972). In previous studies on exocytosis from excitable cells, capacitance measurements were carried out almost exclusively in the hyperpolarized state of the membrane, and contributions from voltage-dependent currents were assumed to be negligible. In pituitary nerve terminals, however, capacitance measurements during depolarization were apparently only weakly contaminated by artifacts from voltage-dependent currents (Lindau et al., 1992), indicating that under appropriate conditions capacitance measurements may be used to monitor exocytotic activity during depolarization.

We investigated the influence of voltage-dependent conductances on capacitance measurements with a lock-in amplifier, and we provide data and formulas to estimate the nature and size of artifacts. These may be used to separate true capacitance changes from the effects of voltage-dependent conductances.

Received for publication 28 December 1994 and in final form 25 September 1995.

Address reprint requests to Dr. Manfred Lindau, Abteilung Molekulare Zellforschung, Max-Planck-Institut für Medizinische Forschung, Jahnstrasse 29, D-69120 Heidelberg, Germany. Tel.: +49-6221-486333; Fax: +49-6221-486325; E-mail: lindau@mzf.mpimf-heidelberg.mpg.de.

0006-3495/95/12/2808/15 $2.00

MATERIALS AND METHODS

Simulation of admittance changes

The admittance of the equivalent circuit of the whole-cell configuration with access resistance R_A, membrane conductance G_M, and membrane

capacitance C_M including the fast capacitance C_F between pipette and bath (see Fig. 1 *A*), was calculated using the following equations:

$$Y_M = \mathrm{Re}(Y_M) + i\mathrm{Im}(Y_M) = G_M + i\omega C_M \quad (1)$$

$$\mathrm{Re}(Z_{WC}) = R_A + \mathrm{Re}(Y_M)/(\mathrm{Re}(Y_M)^2 + \mathrm{Im}(Y_M)^2) \quad (2)$$

$$\mathrm{Im}(Z_{WC}) = -\mathrm{Im}(Y_M)/(\mathrm{Re}(Y_M)^2 + \mathrm{Im}(Y_M)^2) \quad (3)$$

$$\mathrm{Re}(Y_0) = \mathrm{Re}(Z_{WC})/(\mathrm{Re}(Z_{WC})^2 + \mathrm{Im}(Z_{WC})^2) \quad (4)$$

$$\mathrm{Im}(Y_0) = -\mathrm{Im}(Z_{WC})/(\mathrm{Re}(Z_{WC})^2 + \mathrm{Im}(Z_{WC})^2) + \omega C_F \quad (5)$$

$$\mathrm{Re}(Z_0) = \mathrm{Re}(Y_0)/(\mathrm{Re}(Y_0)^2 + \mathrm{Im}(Y_0)^2) \quad (6)$$

$$\mathrm{Im}(Z_0) = -\mathrm{Im}(Y_0)/(\mathrm{Re}(Y_0)^2 + \mathrm{Im}(Y_0)^2) \quad (7)$$

with $\omega = 2\pi\nu$, and ν being the sine wave frequency. Y indicates an admittance, and Z an impedance. Re and Im denote real and imaginary parts. The indices indicate properties of plasma membrane (M), whole cell configuration (WC), and total circuit including C_F (0). In all simulations a sine wave frequency ν = 800 Hz was used. Any change in C_M, G_M, or R_A, or switching the phase tracking resistor R_T into the circuit gives rise to a change in the admittance $\Delta Y = \Delta\mathrm{Re}(Y) + i\,\Delta Im(Y)$ with

$$\Delta\mathrm{Re}(Y) = \mathrm{Re}(Y) - \mathrm{Re}(Y_0) \quad (8)$$

$$\Delta\mathrm{Im}(Y) = \mathrm{Im}(Y) - \mathrm{Im}(Y_0) \quad (9)$$

Simulation of admittance changes detected by a lock-in amplifier

For lock-in capacitance measurements, a sine wave voltage is used as the command signal, and the resulting current is analyzed by the lock-in amplifier. Initially, the lock-in outputs $Y1$ and $Y2$ are at some constant offset denoted $Y1_0$ and $Y2_0$. The command voltage and current output are phase shifted by a certain amount of φ_F, depending on the filters used. When the admittance changes by ΔY, the outputs $Y1$ and $Y2$ of the lock-in amplifier, which is set at the phase $\varphi + \varphi_F$, will then change by a value

$$\Delta Y1 = Y1 - Y1_0 = \frac{\Delta\mathrm{Re}(Y)\cos\varphi - \Delta\mathrm{Im}(Y)\sin\varphi}{|T(\omega)|^2} \quad (10)$$

$$\Delta Y2 = Y2 - Y2_0 = \frac{\Delta\mathrm{Im}(Y)\cos\varphi + \Delta\mathrm{Re}(Y)\sin\varphi}{|T(\omega)|^2} \quad (11)$$

with

$$T^2(\omega) = \frac{1}{(1 + R_A G_M + i\omega C_M R_A)^2} \quad (12)$$

and

$$|T(\omega)|^2 = \frac{1}{(1 + R_A G_M)^2 + (\omega C_M R_A)^2}. \quad (13)$$

With this method the quantities $\Delta Y1$ and $\Delta Y2$ are calibrated in conductance units (*S*). To convert $\Delta Y2$ into capacitance units, the values are divided by ω. The simulation program calculates these signals provided by the lock-in amplifier using Eqs. 1–13, depending on the parameters of the equivalent circuit and the particular phase setting φ. This method can be used when the current-voltage relationship of the membrane conductance is linear.

Simulation of lock-in measurements in the presence of voltage-dependent conductance

When the current-voltage relationship of the membrane conductance is significantly nonlinear in the range covered by the sine wave command signal, admittance calculations as described above are no longer possible because the slope conductance is voltage dependent. The resistor representing membrane conductance in the equivalent circuit should thus be replaced by a voltage- dependent current source $I_M(V_M)$ (see Fig. 1 *B*). The current equation $I = I_M + I_C$ (where I_C represents the capacitive current) leads to the differential equation for the membrane potential V_M:

$$\frac{V_P(t) - V_M(t)}{R_A} = C_M \frac{dV_M(t)}{dt} + I_M(V_M(t)). \quad (14)$$

To simulate lock-in measurements, V_P was assumed to be an 800-Hz sine wave with variable amplitude added to an arbitrary holding potential. V_M was then calculated by integrating Eq. 14 using a fourth-order Runge-Kutta method with adaptive stepsize control (Press et al., 1989). The resulting V_M yielded the pipette current I, which was multiplied with a gain-switch function simulating the lock-in amplifier (Lindau and Neher, 1988). The two lock-in outputs were then averaged over one sine-wave period. For calibration, the change in the $Y2$ channel due to a 200-fF step in C_M was simulated in the same way. For the function $I_M(V_M)$ we used experimentally determined data points (Fenwick et al., 1982; Marty and Neher, 1985; Wang et al., 1992a). The data points were interpolated by a cubic spline or fitted with appropriate functions, and the fitted curves were translated into numerical look-up tables. When the method was applied using a linear *I/V* curve, the results were indistinguishable from those obtained by admittance calculations.

Simulation of lock-in measurements in the presence of voltage-dependent conductance and finite gating kinetics

To account for finite gating kinetics, we assumed first order transitions between an open and a closed state. The time course of the open probability p is described by the differential equation (Hodgkin and Huxley, 1952; Cole, 1972):

$$\frac{d}{dt}p(t) = k(V_M(t)) \cdot (p_\infty(V_M(t)) - p(t)) \quad (15)$$

where $p_\infty(V_M)$ is the voltage-dependent steady-state open probability (activation curve) and $k(V_M)$ is the generally voltage-dependent rate constant. The time course of the membrane current is given by:

$$I_M(t) = p(t) \cdot N \cdot I_0(V_M(t)) \quad (16)$$

with N being the number of channels, and $I_0(V_M)$ the voltage- dependent single-channel current. Together with Eq. 14, this is a complete description of the problem. Integration of the differential equations and simulation of the lock-in amplifier were performed as described above.

Patch clamp recordings

Experiments were carried out using an EPC-9 patch clamp amplifier and a model PAR 5210 (Princeton Applied Research, Princeton, NJ) lock-in amplifier set to a phase of 0°C. An 800-Hz, 20-mV (rms) command voltage was used in all recordings. The lock-in outputs were sampled by a computer equipped with an A/D converter and appropriately phase shifted by the computer program (Lindau, 1991). The bath electrode or a model cell was connected to the ground potential at the head stage of the EPC-9 via a computer-controlled relay, which when opened inserted a 1-MΩ resistor into the ground connection (Fidler and Fernandez, 1989).

Rat peritoneal mast cells were prepared as described and permeabilized by addition of ATP in the whole-cell configuration (Tatham and Lindau, 1990). The recording chamber contained a nominally calcium-free solution of the following composition: 140 mM NaCl, 1 mM $MgCl_2$, 5 mM KCl, 10 mM HEPES/NaOH, and 20 mM glucose (pH 7.2, 305 ± 10 mosm). The intracellular solution (pipette solution) contained 150–160 mM K-glutamate, 7 mM $MgCl_2$, 1 mM K-BAPTA, 100 μM Na_2ATP, and 10 mM HEPES/NaOH (pH 7.2, 290 ± 10 mosm). To permeabilize the cell, 10 μl of bath solution containing 0.5–1 mM ATP was added to the bath close to the pipette tip. The initially high ATP concentration generated a whole-cell conductance around 20–40 nS, which subsequently decayed to a very low level due to dilution by diffusion (Tatham and Lindau, 1990).

RESULTS

Admittance of the whole-cell configuration

The equivalent circuit of the whole-cell configuration including the phase-tracking resistor (R_T) is shown in Fig. 1 *A*. We have included two capacitors contributing to the fast capacitance. The stray capacitance (C_S) is located between the pipette potential and ground, including all grounded metal parts of the setup such as chamber holder and microscope but not bath solution. C_S is always in parallel with the rest of the equivalent circuit and thus always adds a constant value to the admittance. Because we are here only concerned with changes of admittance, the contribution of C_S can be neglected. However, the fast capacitance between the pipette and the bath solution (C_F) is located between the pipette potential and the phase-tracking resistor. When the resistor is switched in, C_F is connected to ground via R_T in series, and the capacitive current through C_F is changed. As shown below, this will affect the accuracy of phase tracking.

Influence of voltage-independent conductance changes on capacitance measurement

The theoretical phase setting of the lock-in where changes in C_M and G_M are best separated is equal to

$$\varphi_0 = -2 \cdot \text{atan}\,[\omega C_M/(1/R_A + G_M)] \qquad (17)$$

which is valid for any value of G_M. Fig. 2 *A* shows the simulation of a linear conductance increase from 0 to 10 nS for a cell with C_M = 6 pF and R_A = 10 MΩ. The lock-in outputs (*solid lines*) show a small reduction in the G trace and a small increase in the C trace even at this correct phase setting. This is due to the fact that the conductance change has a finite size such that the linear approximation for the dependence of the admittance on changes in C_M and G_M is not perfectly valid. Although it was assumed here that the initial G_M is zero and the phase was adjusted accordingly, it should be pointed out that the same increase in the C trace is obtained when the phase setting is defined using G_M = 10 nS in Eq. 17 and the conductance decreases from 10 nS to zero. For the large conductance changes considered here, the quadratic term in the Taylor expansion of the admittance

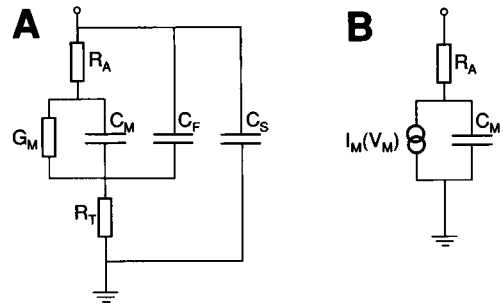

FIGURE 1 (*A*) Equivalent circuit of the patch clamp whole-cell configuration containing membrane capacitance (C_M), membrane conductance (G_M), access resistance (R_A), and phase-tracking resistor (R_T). Stray capacitance (C_S) is located between parts of pipette potential and grounded metal parts of the set-up but not the bath solution. Fast capacitance between pipette and bath (C_F) is located between parts on pipette potential and R_T. (*B*) An equivalent circuit containing a voltage-dependent current source instead of G_M must be used for arbitrary nonlinear current-voltage relationships.

should be considered:

$$\Delta Y \approx \frac{\partial Y}{\partial G_M} \cdot \Delta G_M + \frac{1}{2}\frac{\partial^2 Y}{\partial G_M^2} \cdot \Delta G_M^2 \qquad (18)$$

and the changes of the lock-in outputs become

$$\Delta Y1 \approx \Delta G_M - \frac{R_A}{1 + (C_M R_A \omega)^2} \cdot \Delta G_M^2 \qquad (19)$$

$$\Delta Y2 \approx \frac{C_M R_A^2 \omega}{1 + (C_M R_A \omega)^2} \cdot \Delta G_M^2 \qquad (20)$$

The second-order effect in the C trace is very small. Even for a 10-nS conductance increase, as in the example of Fig. 2 *A*, the C trace changes only by 46 fF (*continuous line*). In Fig. 2 *B*, this cross talk from conductance changes into the capacitance trace, as determined by simulations with the full equivalent circuit admittance, is plotted for different values of C_M and R_A as a function of conductance change on a log-log scale. The linear slopes of ~2 indicate that the effect is indeed mainly proportional to $(\Delta G_M)^2$, reflecting the second-order nature of the phenomenon.

When the phase is misadjusted, much larger artifacts appear in the capacitance trace, as shown for a deviation of 5° in Fig. 2 *A* (*dashed line*). The size of the projections is equal to $\Delta G_M \cdot \sin(\Delta\varphi)/\omega$ and is thus a linear function of ΔG_M. In Fig. 2 *C*, the projections are shown for a 6-pF cell and R_A = 4, 10, and 25 MΩ as a function of ΔG_M, giving a slope of 1 in the log-log plot. The cross talk due to the second-order effect is shown for comparison. For a negative phase error the artifact in the capacitance trace will accordingly be negative.

Phase tracking in the absence of membrane conductance

Experimentally the correct phase setting is approximated during the measurement either by manual variations of the

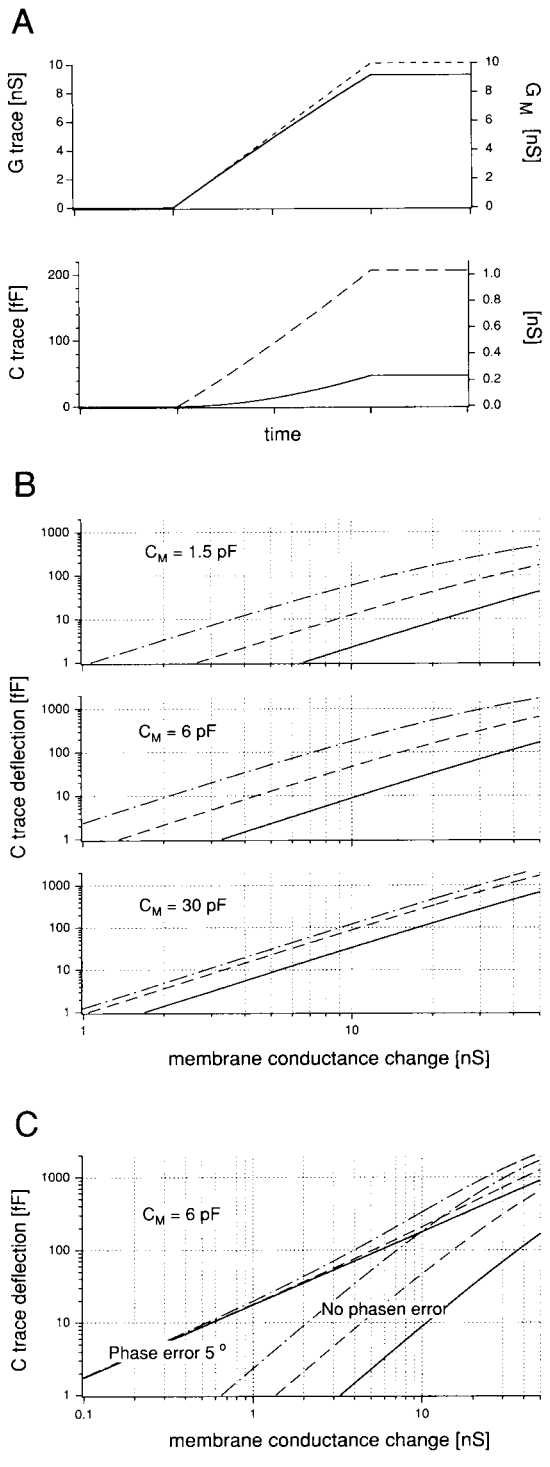

FIGURE 2 (*A*) Simulation of a linear conductance increase from 0 to 10 nS (*dashed line, top*) by admittance calculation for a cell with C_M = 6 pF, R_A = 10 MΩ. In the G trace (*top*), the measured increase (*continuous line*) is slightly less than the true increase (*dashed line*). A small increase occurs in the C trace (bottom panel, continuous line). When the phase is shifted away from the correct setting by 5°, a projection of ~10% occurs in the C trace (*dashed line*), whereas the changes in the G trace are negligible. (*B*) Cross talk from conductance changes into the C trace for various cell parameters. The different lines correspond to R_A values of 4 MΩ (*continuous line*), 10 MΩ (*dashed line*), and 25 MΩ (*dot dashed*). On the log-log scale, slopes are ~2. (*C*) C trace deflections at 5° phase error are much larger, and the slope in the log-log plot is ~1.

capacitance compensation (Neher and Marty, 1982) or by automatic phase tracking, where the phase-tracking resistor R_T is switched into the circuit to simulate a change of R_A (Fidler and Fernandez, 1989). First we examine the accuracy of phase tracking, neglecting C_F for a cell with $G_M = 0$. The impedance of the equivalent circuit is changed according to

$$\mathrm{Re}(Z_T) = \mathrm{Re}(Z_0) + R_T \tag{21}$$

$$\mathrm{Im}(Z_T) = \mathrm{Im}(Z_0) \tag{22}$$

and the admittance correspondingly changes to

$$\mathrm{Re}(Y_T) = \mathrm{Re}(Z_T)/(\mathrm{Re}(Z_T)^2 + \mathrm{Im}(Z_T)^2) \tag{23}$$

$$\mathrm{Im}(Y_T) = -\mathrm{Im}(Z_T)/(\mathrm{Re}(Z_T)^2 + \mathrm{Im}(Z_T)^2). \tag{24}$$

By using the simulation program, we determine the phase obtained by phase tracking and compare it with the optimal phase setting calculated by Eq. 17. An example is shown in Fig. 3 *A* for a 6-pF cell with R_A = 10 MΩ. Initially the phase is set to φ_0 (Eq. 17). When R_T (1 MΩ) is switched in (1), the lock-in output generates a large change in the G trace but also a small negative signal in the C trace, the reason being the finite value of the phase-tracking resistor that leads to a cross talk into the capacitance trace. With the changes

$$\Delta Y1 = Y1(Y_T) - Y1(Y_0) \tag{25}$$

$$\Delta Y2 = Y2(Y_T) - Y2(Y_0) \tag{26}$$

the phase is then adjusted according to

$$\varphi_T = \varphi_0 - \mathrm{atan}(\Delta Y2/\Delta Y1) \tag{27}$$

which in this example is shifted 1.6° from φ_0. When R_T is switched in a second time (2), the deflection in the C trace is eliminated; however, due to the finite size of the phase tracking resistor, the phase setting is shifted away from the correct value. The phase shift obtained with a 1-MΩ resistor is plotted in Fig. 3 *B* as a function of C_M for three different values of R_A (*solid lines*). The effect in the C trace is again mainly a second-order phenomenon due to the quadratic term in the Taylor expansion. The admittance change when R_T is switched into the circuit is

$$\Delta Y = \frac{\partial Y}{\partial R_A} \cdot R_T + \frac{1}{2}\frac{\partial^2 Y}{\partial R_A^2} \cdot R_T^2. \tag{28}$$

At phase setting φ_0, this leads to the lock-in output changes

$$\Delta Y1 \approx (\omega C_M)^2 \cdot R_T \cdot \left(1 - \frac{R_A(\omega C_M)^2}{1 + (\omega C_M R_A)^2} \cdot R_T\right) \tag{29}$$

$$\Delta Y2 \approx -\frac{(\omega C_M)^3}{1 + (\omega C_M R_A)^2} \cdot R_T^2. \tag{30}$$

The phase shift

$$\Delta\varphi = -\mathrm{atan}(\Delta Y2/\Delta Y1) \tag{31}$$

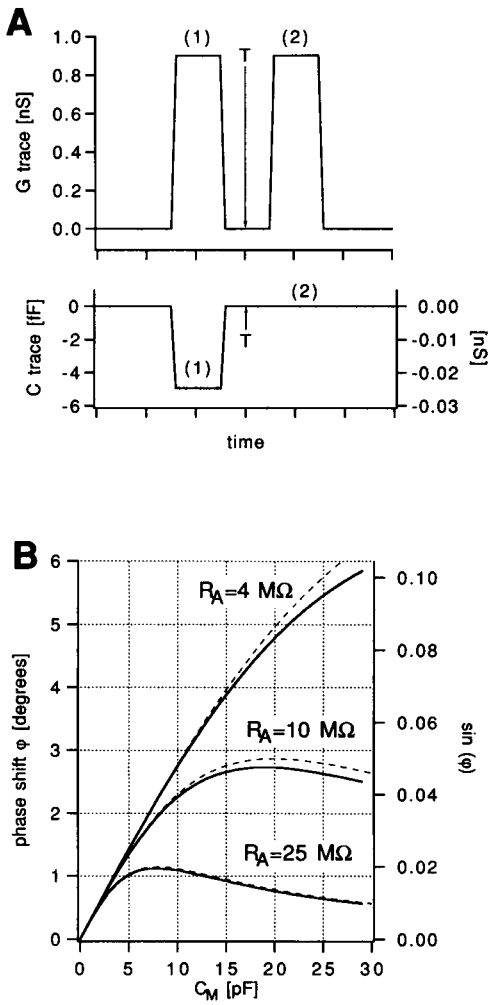

FIGURE 3 (*A*) Simulation of the phase-tracking signals obtained at correct phase setting (1). After phase-adjustment (*T*), the higher order effect in the C trace is eliminated (2), but the phase adjustment is shifted away from the correct value. Cell parameters were C_M = 6 pF, G_M = 0, R_A = 10 MΩ. (*B*) Phase-tracking errors due to higher order cross talks (*continuous lines*) and the approximation by the second-order term (*dashed lines*) for three different values of R_A.

can be approximated by the analytical expression

$$\Delta\varphi \approx \frac{\omega C_M}{1 + (\omega C_M R_A)^2} \cdot R_T \qquad (32)$$

This relationship is shown in Fig. 3 *B* as the *dashed lines*, which in the relevant range are a good estimate of the phase error and can thus be used as a practical equation. According to Eq. 32, the phase error is proportional to the value of the phase-tracking resistor R_T. The phase error would be 10 times smaller if a 100-kΩ resistor were used, but in an actual recording situation the accuracy will be reduced because of the 10 times smaller signal-to-noise ratio. However, because the size of the phase-tracking signal is proportional to $(\omega C_M)^2$ and the phase shift becomes quite large for high capacitance and low R_A (see Fig. 3 *B*), small phase-tracking resistors should be used for cells with high capacitance.

Influence of membrane conductance on phase tracking

In the presence of a significant membrane conductance, the changes in R_A and the changes in G_M occur at different phases (Joshi and Fernandez, 1988). When the phase tracking is simulated for cells with finite membrane conductance, the phase setting is accordingly different from that at which artifacts from conductance changes are minimized. As previously pointed out by Joshi and Fernandez (1988), the theoretical difference between the phase where C trace projections from changes in G_M are minimized and that where C trace projections from changes in R_A are eliminated is

$$\Delta\varphi = 180° - 2\,\mathrm{atan}(\omega C_M/G_M) \cdot \qquad (33)$$

At $(\omega C_M/G_M) < 40$, this phase error $\Delta\varphi$ exceeds 3°, leading to a projection (sin $\Delta\varphi$) of 5% from changes in G_M into the C trace. For a 6-pF cell, a 3° $\Delta\varphi$ corresponds to G_M = 750 pS. To minimize artifacts in the C trace from conductance changes, it is thus important to keep in mind that the phase-tracking method provides a proper phase setting only when it is performed at very low G_M. Otherwise a phase shift $\Delta\varphi$ according to Eq. 33 and a projection proportional to sin$\Delta\varphi$ will occur.

Influence of fast capacitance on phase tracking

We now examine the influence of the fast capacitance C_F, which exists between the pipette and bath solution. The phase-tracking resistor R_T is used to mimic a change of R_A. However, because of the presence of C_F, this change is not exactly equivalent to a change of R_A. Whereas the AC current through the stray capacitance C_S is independent of R_T and can be ignored, C_F does affect the phase tracking as described by Gillis (1995). The value of C_F is typically ~1–2 pF. During phase tracking, the bath and thus also C_F is separated from ground potential by R_T. The contribution of ωC_F to the whole-cell admittance must thus be included (see Eq. 5). The phase-tracking resistor R_T generates a signal with contribution of currents through C_F, and the phase alignment is shifted.

We determined the phase error for C_F = 1 pF and C_F = 2 pF in the computer model for a cell with G_M = 0. The deviations from the ideal phase are plotted in Fig. 4 (*solid lines*) for R_A = 4, 10, and 25 MΩ. The admittance change at first order in R_T is now

$$\Delta Y = \frac{\partial Y}{\partial R_T} \cdot R_T \qquad (34)$$

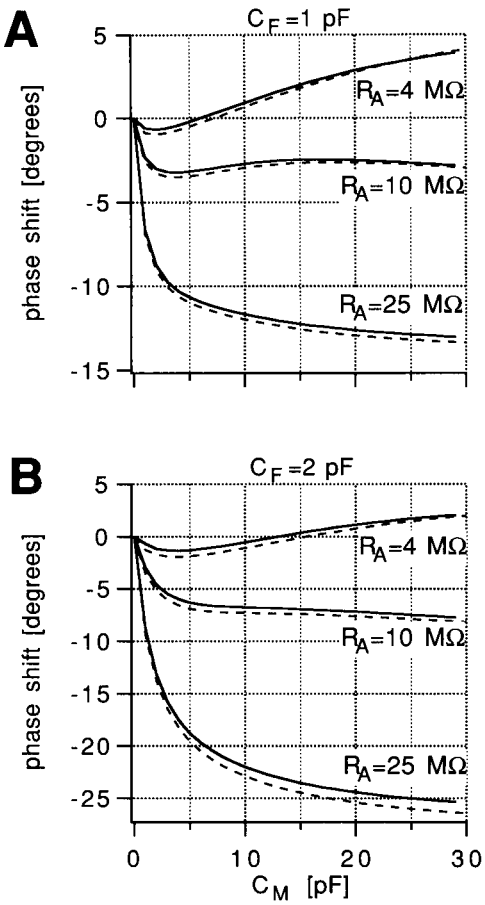

FIGURE 4 Admittance calculations simulating the phase-tracking errors in the presence of fast capacitance (C_F) between pipette and bath, including also the higher order effects for two C_F values typically present when coated pipettes are used.

and at the correct phase setting φ_0 the lock-in output changes are

$$\Delta Y1 = [(C_M + C_F)^2 - (\omega C_M C_F R_A)^2]\omega^2 \cdot R_T \quad (35)$$

$$\Delta Y2 = 2C_M C_F R_A \omega^3 (C_M + C_F) \cdot R_T. \quad (36)$$

The phase error due to C_F at first order in R_T

$$\Delta\varphi = -\text{atan}(\Delta Y2/\Delta Y1) \quad (37)$$

is approximately

$$\Delta\varphi \approx -2\frac{\omega R_A}{1/C_M + 1/C_F}. \quad (38)$$

To obtain the total phase shift, the second-order contribution due to the finite size of R_T (Eq. 30) must be added:

$$\Delta\varphi \approx \frac{\omega C_M}{1 + (\omega C_M R_A)^2} \cdot R_T - 2\frac{\omega R_A}{1/C_M + 1/C_F} \quad (39)$$

The phase shifts obtained with this formula are plotted as dashed lines in Fig. 4. Eq. 39 thus provides a good estimate of the phase error obtained with a 1-MΩ resistor on a cell with $G_M = 0$. The phase shift due to C_F increases with C_M. Because this phase shift has the opposite sign of the second-order effect, both effects initially compensate each other to some extent. At $R_A = 4$ MΩ, the accuracy of the phase tracking is thus generally improved. At high values of R_A, however, the phase error becomes quite large. At $C_F = 2$ pF and $R_A = 25$ MΩ (Fig. 4 *B*), the phase error in a 30-pF cell exceeds 25° and is as high as 18° in a 5-pF cell. To minimize the projection between the C and G traces, this effect should be corrected for. The size of C_F can be estimated when the fast capacitance is first compensated on the patch clamp amplifier before the pipette is immersed into the bath and again later when the seal is formed. The increase in the fast capacitance is a good estimate of C_F as defined by the equivalent circuit of Fig. 1. It should be noted that the phase shift due to C_F given in Eq. 38 and the phase shift due to a significant membrane conductance given in Eq. 33 are not simply additive.

We also investigated the effects of a possible capacitance in parallel to R_T (Gillis 1995), which may be contributed by the switch itself and in addition from a capacitance between the recording chamber and grounded parts such as its holder and the microscope objective. This capacitance can be estimated by connecting the bath electrode to the head stage input connector. When this capacitance is kept low (e.g., ~5 pF as estimated by Gillis (1995)), the additional phase shift is usually <1°, and Eq. 39 may be used to estimate the phase error. However, when the capacitance between the recording chamber and grounded metal parts is large, the more complete equation including this capacitance (Gillis, 1995) must be used. It should be noted that the phase error due to the capacitance in parallel to R_T has a sign opposite to that generated by C_F (Eq. 38) and thus tends to partly compensate for the phase error due to C_F.

Experimental verification of the theoretical analysis

To test the predictions of the above analysis, experiments with various model circuits were performed. By using a model cell with $C_M = 4.7$ pF, $G_M = 0$, and $R_A = 10$ MΩ, phase tracking was performed in the presence and absence of a parallel C_F of 2.2 pF. In the presence of C_F, the fast capacitance compensation indicated an increase of 3.5 pF. Phase tracking with the 1-MΩ resistor using the model circuits with and without C_F revealed a phase shift due to C_F of 10°. This value is very close to the value of 11° predicted by admittance calculations. When C_M was replaced by a 10-pF capacitor, the measured and expected phase shifts were 11° and 14°, respectively.

To determine the accuracy of phase tracking in the absence of C_F, we added a 64-MΩ resistor, corresponding to $G_M = 15.7$ nS in parallel to C_M (4.7 pF), and measured the changes in the C and G trace. The change in the G trace was 13.7 nS, as expected from Eq. 19. However, the measured

change in the C trace was 680 fF (3.4 nS), whereas a change of only 150 fF was expected by the simulation program because of phase-tracking error and the second-order effect. We attribute this discrepancy to stray capacitances of the resistor and connecting wires.

To test the results obtained from theoretical analysis and the model circuits on real recording conditions, we performed whole-cell recordings on rat peritoneal mast cells. In these cells a large nonselective conductance is reversibly induced in the plasma membrane by externally applied ATP (Tatham and Lindau, 1990). Fig. 5 shows such a recording at a holding potential of +40 mV. Cell parameters were C_M = 6.2 pF and R_A = 7.5 MΩ. Phase tracking was performed before permeabilization, when G_M was negligible. When ATP was added to the bath solution close to the cell (t = 0), a large outward current (*top trace*) and a conductance increase (*middle trace*) were observed followed by a subsequent decrease due to dilution of ATP in the recording chamber and formation of the Mg-ATP complex. The DC current and the conductance change with very similar time course and a plot of I versus G had a slope of ~40 mV as expected.

The C trace shows an initial increase followed by a decrease. A net capacitance decrease by ~500 fF, which was still present when the membrane lesions had resealed, indicates that a true capacitance change occurred during the permeabilization period.

The peak conductance was 27.8 nS. From the higher order effects, a cross talk is expected to generate a 260-fF (1.3 nS) increase in the C trace. The estimated value of C_F was ~1.5 pF, generating a phase error of −3.1°, which should lead to a −1.5 nS or −300 fF projection. The expected change in the C trace is thus −40 fF. The maximum value in the capacitance trace was ~620 fF. However, the sustained decrease shows that the permeabilization was also generating true capacitance changes presumably due to changes in exo-endocytotic activity. It is thus not possible with this kind of experiment to separate exactly the effects from conductance and capacitance changes. It should be noted that the measured changes in the C trace are <10% of those in the G trace. Such small capacitance changes in the presence of 10 times larger changes in the conductance trace are thus difficult to interpret when the phase tracking technique is used.

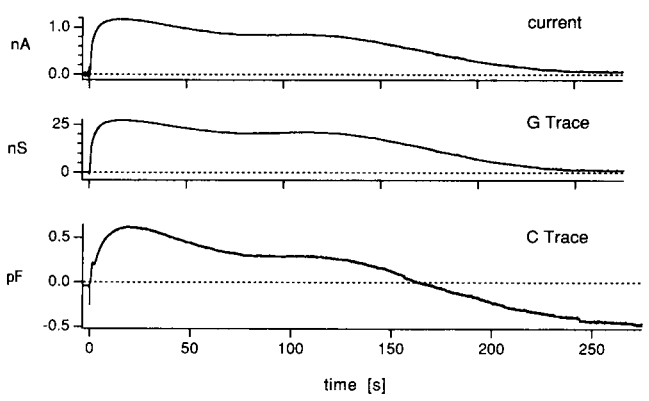

FIGURE 5 Whole-cell lock-in recording of a rat peritoneal mast cell transiently permeabilized by extracellular ATP. *Top*: whole cell DC current; *middle*: conductance change; *bottom*: capacitance change.

Influence of nonlinear conductance changes with non-zero reversal potential

The conductances that may be activated in the cell membrane will usually be due to ion selective channels with a reversal potential different from zero. In addition, the current-voltage relationship will generally be nonlinear. However, the effect detected by the lock-in depends only on the properties of the conductance in the range of the sine wave voltage. If the sine wave amplitude is small (e.g., <20 mV), then the current-voltage relationship in this range may in many cases be well approximated by a straight line. A non-zero reversal potential adds only a DC current, which is not affecting the lock-in measurement. The slope conductance is thus the quantity to be used in the equivalent circuit of Fig. 1, independent of the reversal potential.

In some cases the current-voltage relationship may not be well approximated by a straight line, as for example for calcium channels between −10 and +20 mV, where the *I/V* curve goes through a minimum. Because activation of voltage-dependent calcium channels is of particular importance in studies on exocytosis, we investigated the effects of these currents in more detail. As a most interesting example we used the voltage-dependent calcium current in bovine chromaffin cells for two reasons. First, the chromaffin cell is the system most widely used to study calcium-dependent exocytosis; second, for this cell type an excellent detailed description of the voltage-dependent properties is available (Fenwick et al., 1982). To investigate the influence of nonlinear conductances we replaced the membrane conductance G_M by a voltage-dependent current source $I_M(V_M)$ (Fig. 1 *B*). The membrane potential determining I_M was calculated by numerical integration of Eq. 14. For the function $I_M(V_M)$, the experimentally determined *I/V* curve of the isolated calcium current in bovine chromaffin cells (Fenwick et al., 1982) was used (Fig. 6, *top*). The resulting lock-in signals were calculated by the simulation program for a 6-pF cell with 10-MΩ access resistance.

The middle panel shows the slope conductance (*continuous lines*) and the lock-in signals obtained from the simulations for a 2-mV (*diamonds*) and a 20-mV (*circles*) sine wave. These points are very close to the slope conductance curve, indicating that the slope conductance at the holding potential is the main factor determining the conductance signal even in the presence of significant nonlinearity.

The bottom panel shows as a continuous line the cross talk predicted by admittance calculations for linear conductances equal to the slope conductances shown in the corresponding conductance panels. The points obtained for the 2-mV sine wave amplitude agree perfectly well with this

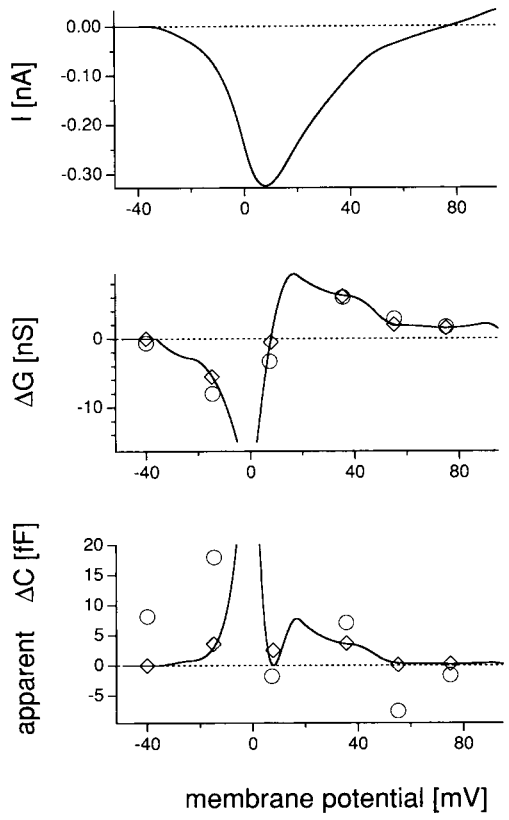

FIGURE 6 Numerical calculation of the signals measured by a lock-in amplifier in the presence of nonlinear current-voltage relationships. *Top*: *I/V* curve of whole-cell calcium current in bovine chromaffin cells; *middle*: slope conductance (*continuous line*) and simulated lock-in changes in G trace for a 2-mV (*diamonds*) and 20-mV (*circles*) sine wave amplitude; *bottom*: cross talk calculated from slope conductances (*continuous line*) and simulated changes in the C trace (*diamonds, circles*).

curve because in this range the corresponding part of the *I/V* curve is well approximated by a straight line. A deviation occurs for the 20-mV sine wave, when the mean conductance in the range of the sine wave is significantly different from the conductance at the holding potential. The cross talk may now even be negative, but its size is still in the range obtained for linear conductances with a size similar to that present within the sine wave amplitude. It should be noted that in Fig. 6 the membrane potential rather than the pipette potential is plotted on the abscissa to obtain a proper conversion of the *I/V* curves. The voltage drop across the pipette resistance can be estimated from the size of the holding current at a particular membrane potential.

The simulations were also performed for three other experimentally determined *I/V* curves (results not shown): the calcium-dependent K current as measured in pituitary nerve terminals (Wang et al., 1992a) and the whole-cell currents measured in bovine chromaffin cells in the absence and presence of extracellular calcium (Marty and Neher, 1985). In all cases the agreement with the slope conductance was even better than in the case of Fig. 6 because the isolated calcium current shows the strongest nonlinearity.

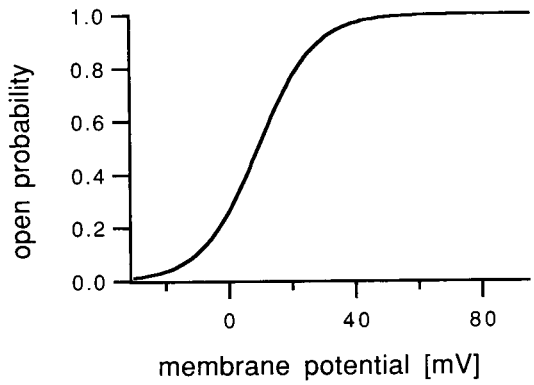

FIGURE 7 Activation curve fitted to data points taken from Fenwick et al. (1982). Fit function was a Boltzmann-type curve

$$p_\infty(V_M) = \frac{1}{1 + k_1 e^{-k_2 V_M}}.$$

Best fit was obtained with $k_1 = 2.822$ and $k_2 = 0.1123\ \text{mV}^{-1}$.

Simulation of lock-in measurements in the presence of gating kinetics

Voltage-dependent channels do not react to changes of the membrane potential instantaneously, and it is well known that this behavior leads to frequency-dependent, phase-shifted currents in response to a sinusoidal voltage (Cole, 1972). To investigate the effect of gating kinetics on capacitance measurements with a lock-in amplifier, we used a simple kinetic model assuming transitions between an open and a closed state according to first-order kinetics

$$\text{Close} \underset{k_1}{\overset{k_2}{\leftrightarrows}} \text{Open},$$

with k_1 and k_2 being the rate constants. The time dependence of the open probability p is described by Eq. 15, with the voltage-dependent steady-state open probability

$$p_\infty = \frac{k_1}{k_1 + k_2}$$

and the voltage-dependent rate constant $k = k_1 + k_2$. In the most simple case of a linear-current voltage relationship of the open channel with zero reversal potential and single-channel conductance G_0, the membrane current I_M can be written as

$$I_M(t) = p(t) N G_0 V_M(t) \qquad (40)$$

with N being the number of channels.

For simplicity, we first assume a fixed (voltage-independent) time constant and a Boltzmann-type activation curve. The activation curve was fitted to the experimental values of the plateau current of voltage-dependent calcium channels in bovine chromaffin cells (Fenwick et al., 1982) (Fig. 7).

The finite kinetics of voltage-dependent channels generate a phase shift of the membrane current (Cole, 1972). This phase shift leads to changes in the C trace, in addition to the effects described before.

Fig. 8 shows the simulated signals in G trace and C trace for the activation of a linear membrane conductance with 0 mV reversal potential (Eq. 40) as a function of the rate constant k. Cell parameters were R_A = 4 MΩ, 10 MΩ, and 25 MΩ, C_M = 6 pF, and NG_0 = 20 nS. The depolarization potential was assumed to be +20 mV, and the sine wave amplitude was ± 20 mV.

The largest effect in the C trace occurs at $k \approx 5000\ s^{-1}$, corresponding to the angular frequency of the sine wave. For small k values (slow kinetics), the open probability cannot follow the variations of the membrane potential and is therefore basically constant. The C signal is then reduced to the higher order cross talk, which can be approximated by admittance calculations. For example, for R_A = 4 MΩ and $k = 10\ s^{-1}$, the mean conductance determined in the simulation was 13.5 nS. In admittance calculations, this yields a 12.8-nS signal in the G trace and a 15.5-fF signal in the C trace (*open circles* in Fig. 8). The simulations including the kinetics give 12.8 nS and 13.2 fF, respectively, which is in excellent agreement with the admittance calculations.

At very high kinetic rates k, the open probability immediately follows the sine wave. The results can then be obtained by using the method of voltage-dependent channels without kinetics, as described above with the *I/V* curve given by Eq. 40. The values obtained with this method are indicated as *filled circles* in Fig. 8 and are in excellent agreement with those that are obtained when the kinetics are taken into account.

To separate the contributions of the different effects in the C trace (higher order cross talk and finite kinetics) and to obtain error formulas, approximate analytical expressions were derived. We assumed that the membrane potential is composed of a sine wave and a constant offset

$$V_M(t) = V_M^H + V_M^0 \sin(\omega t) \tag{41}$$

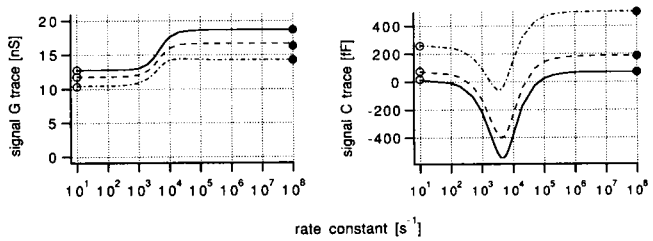

FIGURE 8 Results from simulations with variable but voltage-independent rate constants (Eqs. 40, 14, and 15) using C_M = 6 pF and NG_0 = 20 nS. The curves are for R_A = 4 MΩ (*solid line*), 10 MΩ (*dashed line*) and 25 MΩ (*dash dotted line*). Open circles at the left of the panels show the results from admittance calculations as an approximation for small rates. For these calculations the mean membrane potential and mean membrane conductance determined in the full simulation were used. Filled circles on the right indicate values obtained with the method for voltage-dependent channels without kinetics.

and the electromotive force (emf) E may then be approximated as

$$E(t) = V_M^H - V_{rev}^* + V_M^0 \sin(\omega t) \tag{42}$$

where V_{rev}^* is the extrapolated reversal potential of the single channel current I_0 at the holding potential, i.e., the intercept between the tangent of the open channel *I/V* curve at V_M^H with the current axis:

$$V_{rev}^* = V_M^H - \frac{NI_0(V_M^H)}{\left.\frac{\partial(NI_0(V_M))}{\partial V_M}\right|_{V_M = V_M^H}}. \tag{43}$$

Neglecting the voltage dependence of the single-channel conductance G_0 within the range of the sine wave, i.e., assuming that the single channel *I/V* is linear in this range, the membrane current can be written as the product of emf, number of channels, single-channel conductance, and open probability:

$$I_M(t) = NI_0(V_M(t))p(t) \approx E(t)NG_0(V_M^H)p(t). \tag{44}$$

Although this is only an approximation, inasmuch as G_0 may be generally voltage dependent because of nonlinearity of the single channel *I/V* curve, this nonlinearity will be rather small in many cases.

For an analytical treatment, the activation curve must also be linearized around the pipette holding potential V_H in the range of the command voltage:

$$\begin{aligned} p_\infty(V_H + \Delta V) &= p_\infty(V_H) + \Delta V \left.\frac{\partial}{\partial V'} p_\infty(V')\right|_{V' = V_H} \\ &= \beta + \alpha \Delta V \end{aligned} \tag{45}$$

with the parameters:

$$\alpha = \left.\frac{\partial}{\partial V'} P_\infty(V')\right|_{V' = V_H} \qquad \beta = p_\infty(V_H) \tag{46}$$

With these assumptions, the differential equation (Hodgkin and Huxley, 1952; Cole, 1972)

$$\frac{d}{dt} p(t) = k(V_M(t)) \cdot (p_\infty(V_M(t)) - p(t)) \tag{15}$$

can be rewritten as:

$$\frac{d}{dt} p(t) = k(\beta + \alpha V_M^0 \sin(\omega t) - p(t)) \tag{47}$$

where the voltage dependence of the rate constant k was neglected within the range of the sine wave.

Eq. 47 can be solved analytically, and the open probability can be written as a function of time:

$$p(t) = \beta + \alpha V_M^0 \frac{(k^2 \sin(\omega t) - k\omega \cos(\omega t))}{k^2 + \omega^2}. \tag{48}$$

The transient part of the open probability that vanishes

exponentially with t has been omitted. The first part of the sum (β) is the steady-state open probability at the mean membrane potential and represents a linear conductance. The second part ($\propto \alpha V_M^0$) is the variation of the open probability caused by the sinusoidal part of the membrane potential.

The membrane current can be written as the product of emf and conductance:

$$I_M(t) = NG_0 p(t)E(t)$$

$$= NG_0\left(\beta + \alpha V_M^0 \frac{(k^2 \sin(\omega t) - k\omega\cos(\omega t))}{k^2 + \omega^2}\right) \quad (49)$$

$$\times (V_M^H - V_{rev}^* + V_M^0 \sin(\omega t))$$

By factoring out, constant terms as well as terms with frequencies ω and 2ω appear. Because the lock-in amplifiers measure at ω, only terms with this frequency have to be taken into account:

$$I_M^\omega = NG_0 V_M^0\left(\beta \sin(\omega t) + \alpha(V_M^H - V_{rev}^*)\right.$$

$$\left.\times\left(\frac{k^2}{k^2 + \omega^2}\sin(\omega t) - \frac{k\omega}{k^2 + \omega^2}\cos(\omega t)\right)\right) \quad (50)$$

The first term results from the constant part of the open probability. The term proportional to α results from the product of the constant part of the emf and the sinusoidal variation of the membrane conductance. Here, the current varying with the sine is in phase with the ohmic current, whereas the cosine term contributes an apparent capacitive current. Because of the kinetics, the lock-in amplifier thus measures an apparent conductance and capacitance in addition to the cross talk from the mean conductance:

$$\Delta G_{kin} = NG_0\alpha(V_M^H - V_{rev}^*)\frac{k^2}{k^2 + \omega^2}$$

$$\omega\Delta C_{kin} = -NG_0\alpha(V_M^H - V_{rev}^*)\frac{k\omega}{k^2 + \omega^2} \quad (51)$$

Similar results were derived for the contribution of voltage-dependent currents to the conductance and capacitance in the Hodgkin-Huxley Axon using a linearization approach (Cole, 1972). Fig. 9 *A* shows these expressions as a function of k in normalized units. To estimate V_M^H, we approximate:

$$V_M^H = \frac{V_H + R_A\beta G_0 V_{rev}^*}{1 + R_A\beta G_0} \quad (52)$$

where V_H is the holding potential at the pipette. This expression is not exact, inasmuch as the variations of the membrane conductance have been neglected. Furthermore, if V_M^H differs markedly from V_H, then α and β (Eq. 46) should be recalculated using V_M^H instead of V_H. This may be repeated in an iterative manner until V_M^H is stable.

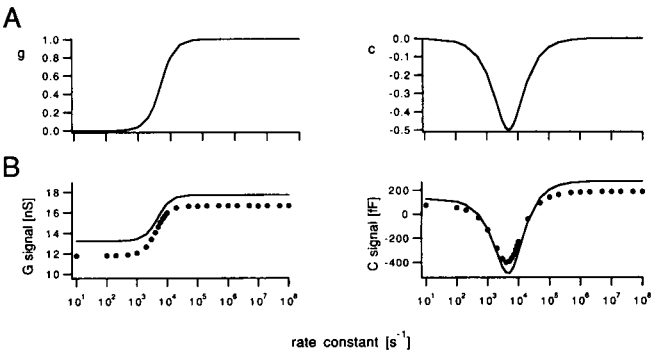

FIGURE 9 (*A*) Normalized signals (Eq. 51) in G trace (*left*) and C trace (*right*) caused by variation of open probability.

$$g = \frac{\Delta G_{kin}}{\alpha V_M^H NG_0}, \qquad c = \frac{\Delta C_{kin}}{\alpha V_M^H NG_0}.$$

(*B*) Signals in G trace and C trace of the lock-in amplifier from numerical simulation as in Fig. 8 (*dots*) and analytical approximation according to Eq. 53 (*continuous lines*). Cell parameters were R_A = 10 MΩ, C_M = 6 pF, and NG_0 = 20 nS.

With these expressions, lock-in outputs can be calculated according to Eqs. 19 and 20:

$$\Delta Y_1 = \beta G_0 + \Delta G_{kin} - \frac{R_A}{1 + (C_M R_A\omega)^2}(\beta G_0 + \Delta G_{kin})^2$$

$$\Delta Y_2 = \omega\Delta C_{kin} + \frac{C_M R_A^2\omega}{1 + (C_M R_A\omega)^2}(\beta G_0 + \Delta G_{kin})^2 \quad (53)$$

Fig. 9 *B* shows the values obtained by integrating the differential equations (*dots*) in comparison with the values estimated by Eq. 53 (*continuous line*). Obviously, these equations provide a good approximation for the effects caused by the finite kinetics of voltage-dependent channels.

Simulation of voltage-dependent calcium currents including kinetics

In general, the time constant and the slope conductance of the open channel will both depend on membrane potential. To account for these effects, simulations were carried out using the properties of the isolated calcium current in chromaffin cells (Fenwick et al., 1982) depicted in Fig. 10. The instantaneous current-voltage relationship NI_0 (Fig. 10 *A*) was derived from a polynomial fit to the data points of Fenwick et al. (1982) and was used together with the steady-state *I/V*-curve (Fig. 6, *top*). To calculate the voltage dependence of the open probability (Fig. 10 *B*) below 43 mV, we used NI_0 and the macroscopic *I/V*-curve. Above 43 mV, the open probability was set to p = 1, and NI_0 was assumed to be reflected in the macroscopic *I/V*-curve.

The kinetics of the calcium current does not follow simple first-order kinetics, and the description with a single time constant as assumed here is only an approximation. The relevant mean relaxation rate should ideally be measured by using small voltage steps in the range of the sine

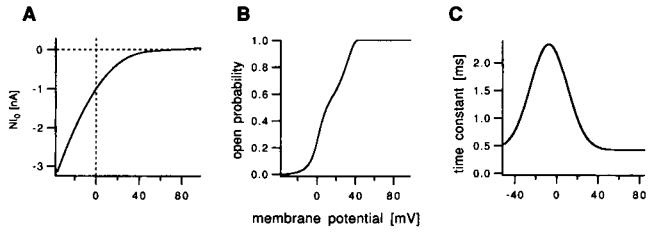

FIGURE 10 Voltage-dependent properties used for realistic simulations of a voltage-dependent calcium current, taken from Fenwick et al. (1982). (*A*) Current voltage relationship with all channels activated. (*B*) Voltage dependence of open probability. This curve was generated such that the combination with the curve of *A* gives the *I/V* curve shown in Fig. 6. (*C*) Voltage dependence of time constant. The data points from Fenwick et al. (1982) were fitted with a gaussian function with

$$\tau(V_M) = \tau_0 + \tau_1 \exp\left(-\frac{V_M - V_{Max}}{\sigma_\tau}\right).$$

with $\tau_0 = 0.425$ ms, $\tau_1 = 1.91$ ms, $V_{Max} = -7.46$ mV, and $\sigma_\tau = 25.0$ mV.

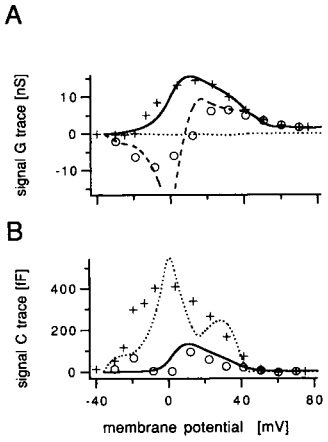

FIGURE 11 Results of simulations with voltage-dependent calcium current. Crosses give the simulated signals using channel properties from Fig. 10. Circles give results for an infinitely fast kinetic, using the *I/V* curve from Fig. 6. In *A*, the dashed line is the slope of the *I/V* curve from Fig. 6. The continuous line gives the slope of the *I/V* curve of Fig. 10 *A*, multiplied by the steady-state open probability. The solid line in *B* is the theoretical second-order cross talk corresponding to this conductance. Cell parameters were $R_A = 10$ MΩ and $C_M = 6$ pF. The contributions due to channel kinetics (Eq. 51) are shown as dotted lines.

wave around the respective membrane potential. Unfortunately, a complete data set of this kind is not yet available. We thus used the activation and deactivation kinetics as measured by Fenwick et al. (1982). Activation occurs with a strongly voltage-dependent time constant (Fenwick et al., 1982), which could be fitted by a Gaussian function (Fig. 10 *C*). The activation is preceded by a weakly voltage-dependent delay of ~200–400 μs, and a similar time constant is present as a fast component in the tail-current decay (Fenwick et al., 1982). However, at potentials close to 0 mV, the delay is negligible compared with the rising phase of the current, and its amplitude in the tail current approaches zero for transitions between 0 and −10 mV (Fenwick et al., 1982). The fast component was thus neglected to keep the analysis simple. The simulation of the calcium current is thus only an approximation but should be a very good one in the most interesting range around 0 mV membrane potential. Deviations may occur at negative potentials where larger contributions from the fast component may be expected. However, at −40 mV, the two time constants differ only by a factor of 2, which will also keep the error small.

The results of the simulations are shown in Fig. 11. Cell parameters were $R_A = 10$ MΩ and $C_M = 6$ pF. In Fig. 11 *A*, the *crosses* show the simulated signals in the G trace as a function of membrane potential. The *dashed line* shows the slope conductance of the whole-cell Ca current given in Fig. 6 (*top*), i.e., assuming infinitely fast kinetics and infinitely small sine wave amplitude. This curve agrees quite well with the results of the simulation with infinitely fast kinetics, including the full sine wave amplitude (*circles*), but both are obviously completely wrong in comparison with the results using the finite channel kinetics. In contrast, the continuous line was obtained assuming infinitely slow kinetics and infinitely small sine wave amplitude, i.e., the conductance at a given holding potential was simply calculated as the slope of Fig. 10 *A* multiplied by the open probability given in Fig. 10 *B*. This line is in good agreement with the conductance values from the full simulation reflecting the fact that in the range where the open probability varies significantly with voltage, the time constant is always significantly slower than the 200 μs value corresponding to the 800-Hz sine wave. It should be noted that the AC conductance measured at 800 Hz is always positive even in the range where the slope conductance of Fig. 6 (*top*) is steeply negative (between −20 and +5 mV). The reason is that because of the slow kinetics the open probability is almost constant, and the *I/V* relationship seen by the sinusoidal membrane potential is determined by the voltage dependence of the open-channel current, which has a positive slope multiplied by the open probability at the holding potential. At +3.8 mV, the open probability is ~0.35, and the slope conductance of the open channels NG_0 as determined from tail currents is 37.4 nS (see Fig. 10). The resulting 13.2 nS are in good agreement with the value of 13.1 nS determined in the simulation.

The correlated effect in the C trace (*crosses* in Fig. 11 *B*), however, is significantly larger than that estimated as the second-order cross talk using conventional admittance calculations (*continuous line*). The cross talk into the C trace should be be <150 fF, and this is actually obtained when 10 times slower kinetics are assumed for the calcium current (data not shown). The additional effect is thus due to the finite kinetics. In contrast to Fig. 8, the additional signal in the C trace is positive because the calcium current is negative (inward). It thus adds to the cross talk in the same direction. The contributions from finite channel kinetics (Eq. 51) are shown as *dotted lines* in Fig. 11. Around 0 mV,

the condition $k^2 \ll \omega^2$ is fulfilled and Eq. 51 may be simplified to

$$\Delta G_{kin} = NG_0\alpha(V_M^H - V_{rev}^*)\left(\frac{k}{\omega}\right)^2$$
$$\omega\Delta C_{kin} = -NG_0\alpha(V_M^H - V_{rev}^*)\frac{k}{\omega} \quad (54)$$

or when the current through the open channels at the holding potential $I_0(V_M^H)$ is used:

$$\Delta G_{kin} = N\alpha I_0(V_M^H)\left(\frac{k}{\omega}\right)^2$$
$$\omega\Delta C_{kin} = -N\alpha I_0(V_M^H)\frac{k}{\omega}. \quad (55)$$

The contribution of the kinetic effect to the conductance ΔG_{kin} is thus scaled approximately with $(k/\omega)^2$, which is $\sim$0.01 around 0 mV where τ is $\sim$2 ms.

For the effect in the C trace $\omega\Delta C_{kin}$, however, the scaling factor is approximately $k/\omega \approx 0.1$, 10 times larger than that for the G signal. The average slope α of the activation curve (Eq. 46) is $\sim$0.02 mV^{-1} (Fig. 10 *B*), and the current through the open channels at 0 mV membrane potential is ~ -1 nA. Eq. 55 thus yields $\Delta G_{kin} \approx -0.2$ nS and $\omega\Delta C_{kin} \approx +2$ nS or $\Delta C_{kin} \approx 400$ fF, in good agreement with the results of the simulation (Fig. 11). Eqs. 51, 54, and 55 thus make possible an easy quantitative estimate of the kinetic effects on the measured capacitance changes. It should be noted that comparatively large changes occur at membrane potentials around -20 mV. This is probably due to the strong bending of the activation curve in this range (Fig. 10 *B*) such that the sine wave picks large contributions when it is in the positive range. The effect was not observed when a 2-mV sine wave was used in the simulation.

CONCLUSIONS

We analyzed the distortion of capacitance measurements with a lock-in amplifier generated by large conductance changes in the plasma membrane. At correct phase setting, a voltage-independent conductance generates a cross talk mainly due to second order effects, which can easily be estimated by using Eq. 20. The phase-tracking technique using a 1-MΩ resistor switched into the ground connection may be used to adjust the phase when membrane conductance is low. However, even then the phase obtained with this method may be wrong because of second-order effects and the influence of the fast capacitance of the pipette tip. For the phase-tracking errors, similar equations were derived by Gillis (1995). This author also included a switch capacitance in parallel to the phase-tracking resistor, which will be mainly generated between the bath on one side and the metal parts of the holder and microscope on the other side. This capacitance leads to a phase shift with a sign opposite to that of the phase shift due to the fast capacitance of the pipette tip and may partly compensate the effect of pipette-tip capacitance. When the capacitance between recording chamber and ground is <5 pF, its contribution to the phase shift is usually <1°. For larger values the phase error will usually be smaller and should be estimated using the more complete formula given by Gillis (1995).

In most cases the phase-tracking error $\Delta\varphi$ will be <15°. The projection from conductance or access resistance changes into the capacitance trace in this range are proportional to sine ($\Delta\varphi$). The size of possible artifacts can thus be estimated. Capacitance changes in the range of these artifacts must be treated with caution, and the accuracy of phase setting must be confirmed separately. For capacitance measurements with a lock-in amplifier, it is thus very important that both traces are displayed at corresponding gain, i.e., for the widely used 800-Hz sine wave frequency, a 1-pF capacitance change should have the same size as a 5-nS conductance change.

When the conductances and the current-voltage relationships are nonlinear and kinetics are fast compared with the sine wave, the effects in the C trace are more complicated, but the size of the artifacts may still be estimated from the slope conductances present in the range of the sine wave. Voltage-dependent channels do not react to changes in membrane potential instantaneously but react with a finite kinetic rate, which in most cases is slower or similar to the angular frequency of the sine wave. This kinetic effect gives rise to additional effects that are maximal when the rate constant is close to the angular frequency of the sine wave. In whole-cell recordings a frequency of 800 Hz is often used to optimize the signal-to-noise ratio, corresponding to $\omega = 5000\ s^{-1}$ and a characteristic time constant of 200 μs. To account for the kinetics of a voltage-dependent channel, the relaxation times in the range of the sine wave determine the resulting effects and these should thus be determined using small voltage steps.

We approximated the kinetics of the voltage-dependent calcium current in bovine chromaffin cells assuming first-order kinetics using the main activation and deactivation time constant given in Fenwick et al. (1982). Around 0 mV the activation time constant of the Ca current in bovine chromaffin cells is 2.5 ms (Fenwick et al., 1982), more than an order of magnitude slower than the characteristic time constant of the 800 Hz sine wave. At this potential, the open probability thus varies only weakly with the sine wave. The relevant slope conductance seen by the sine wave command voltage is nearly identical to the slope conductance of the open channels multiplied by the open probability at the holding potential (Fig. 11).

The correlated effect in the C trace, however, is significantly larger than that estimated as the second-order cross talk using conventional admittance calculations. If the activation curve and kinetics of the current are known, then the effect of channel kinetics on the capacitance measurements can be estimated, however, by rather simple formulas. In summary, we provide formulas that make it possible to estimate the size of artifacts in the capacitance trace from

voltage-dependent conductances, which may be applied generally.

In a previous study on exocytosis from single nerve terminals, a biphasic capacitance increase was observed during depolarization (Lindau et al., 1992) that consisted of a rapid increase by ~120 fF during the first 100 ms followed by a slow increase at a rate of ~30 fF/s, which lasts several seconds. In these nerve terminals, sodium, potassium, and calcium currents are present. After depolarization to −10 mV, the sodium currents as well as the transient component of the calcium current rapidly inactivate (Lemos and Nowycky, 1989; Wang et al., 1992b). The A-current is completely inactivated within 300 ms after depolarization to near 0 mV (Bielefeldt et al. 1992; Thorn et al. 1991; Kilic and Lindau, unpublished data). Although this conductance will generate additional artifacts during its activation, it does not contribute at times later than 300 ms after the potential change. The main conductance present after this time is a calcium-dependent K current (Wang et al., 1992a). During depolarization a peak conductance of 6–8 nS was measured (Lindau et al., 1992). This current has very slow kinetics ($\tau \approx 100$ ms) (Kilic and Lindau, 1995), and the cross talk may be estimated by using Eq. 20. For a typical nerve terminal with 2.5 pF capacitance and R_A = 10 MΩ, a cross talk <15 fF is expected. In pituitary nerve terminals, calcium currents are small, and after 100 ms only the L-type current remains, which has a peak value of ~20 pA when 2 mM Ca^{2+} is present in the bath solution (Lemos and Nowycky, 1989; Wang et al., 1992b; Stuenkel, 1994). The second-order effect of such a small conductance will be negligible. However, this current may contribute an apparent capacitance signal because of its finite kinetics. Unfortunately, detailed kinetic data are not available for the L-type calcium current of pituitary nerve terminals. However, this current is similar to the calcium current in chromaffin cells and to the noninactivating high-voltage-activated calcium current in presynaptic terminals of the chicken ciliary ganglion (Yawo, 1990). The latter has an activation time constant of ~2.5 ms at +20 mV (Yawo, 1990), and we estimate an activation time constant of ~2 ms at +10 mV for the L-type current in pituitary nerve terminals from recordings shown in Wang et al. (1992b), similar to that in chromaffin cells (Fenwick et al., 1982). The maximal slope of the activation curve in presynaptic nerve terminals is ~0.02 mV^{-1}, and the slope between −10 mV and 0 mV is about 0.01 (Yawo, 1990). For the L-type calcium current in pituitary nerve terminals, it is thus reasonable to assume an activation time constant of ~2 ms and a slope of the activation curve that is <0.02 mV^{-1}. With these estimates and the size of the L-type calcium current in pituitary nerve terminals, we estimate <25 fF apparent capacitance change due to activation of this current. Together with the second-order effect from the calcium-activated K-current, the artifact in the capacitance trace 300 ms after the onset of depolarization should thus be <40 fF.

A phase error of a few degrees, however, will introduce substantial projections in the C trace as seen in Fig. 5 of Lindau et al. (1992). A subsequent phase readjustment of the recorded data was performed minimizing the change in the capacitance trace associated with the conductance decrease during repolarization. At this time the conductance was ~5 nS, and the capacitance was ~2.2 pF. Assuming R_A <12 MΩ, a second-order cross talk <7 fF is expected. Together with the kinetic effect from the calcium current, an apparent capacitance change <32 fF may thus occur during repolarization. Accordingly, eliminating the step in the capacitance trace by phase adjustment may result in a phase error < atan($\omega \cdot$ 30fF/5nS) < 2°. These estimates indicate that the error relative to the measured total capacitance increase of ~300 fF was probably <10%. Because during depolarization the bulk conductance varied only within a factor of 2 and the contribution from noninactivating calcium current should be constant, the corresponding apparent change in the capacitance measurement should also be almost constant during the depolarization. Its contribution to the initial step accordingly may be as much as 30%. However, the offset in the capacitance trace during depolarization should be almost constant and may have been partly compensated for by eliminating the shift at the end of the depolarization by the method of phase adjustment.

This may explain why it was possible to observe the rapid exocytotic burst followed by a slow phase of exocytosis during depolarization. Accordingly, a slightly smaller exocytotic burst was observed when nerve terminals were depolarized for <100 ms, and capacitance was measured in the hyperpolarized state (Lindau et al., 1992). Evidence for a rapid exocytotic burst during depolarization was also obtained in chromaffin cells (Augustine and Neher, 1992). Also, in the absence of depolarization, i.e., in the absence of voltage-dependent currents, two or even more kinetic phases of exocytosis were characterized by using stepwise calcium changes from photolysis of a light-sensitive calcium chelator (Neher and Zucker, 1993; Thomas et al., 1993a,b; Heinemann et al., 1994). All of these results strongly support the existence of a small rapidly releasable pool of vesicles.

The problem that large linear conductance changes generate apparent changes in the capacitance trace may be avoided when a third parameter such as the DC conductance (Lindau and Neher, 1988) is measured. This technique is clearly superior because it completely avoids the problems of a possible phase error, as well as the second-order cross talk from large conductance changes into the capacitance measurement. However, for voltage-dependent currents, even this method cannot completely eliminate artifacts in the capacitance measurements.

The voltage-dependent calcium current is a good example to illustrate the difficulties. Because at a typical depolarization potential of 0 mV the kinetics is slow, the

conductance is determined by the voltage dependence of the open-channel current and the number of open channels at the given membrane potential. In this case the conductance thus cannot simply be calculated from the DC current and the reversal potential. The kinetic effects due to phase-shifted currents will also be present. We have not yet analyzed the influence of voltage-dependent conductances on capacitance measurements with this method in a quantitative manner. However, in principle the effects will be similar, except that the cross talk and phase problems do not occur. Eqs. 51, 54, and 55 should also be applicable with this technique.

More recently, it was proposed that simultaneous application and analysis of two sine waves with different frequencies may be used to separate changes in conductance, capacitance, and series resistance (Rohlicek and Rohlicek, 1993; Donelly 1994; Rohlicek and Schmid 1994). It was demonstrated that with this method the cross talk from large conductance changes into the capacitance trace is very small (Rohlicek and Schmid 1994), but the noise level in the capacitance measurement is about two times larger (Gillis 1995). For the example of voltage-dependent calcium currents given here, the contribution from channel kinetics to the currents at the different frequencies will be different at the two frequencies and may thus potentially provide even more information to estimate the contribution from voltage-dependent conductances. Another approach might be to use a wide range of frequencies simultaneously, such as a pseudo-random binary sequence (Clausen and Fernandez 1981), white noise (Moore and Christensen 1985), or a voltage square pulse (Lindau and Neher 1988). Although in principle these latter techniques may be able to separate currents on the basis of their kinetics, they suffer from low resolution in capacitance as well as time and may not be applicable to detect small or fast capacitance changes.

Measurements with a lock-in amplifier provide two quantities: the time course of apparent conductance and the time course of apparent capacitance. The activation of large conductances may lead to significant projections into the capacitance measurement when the phase-tracking technique is used. These may be mistaken as exo-endocytotic phenomena or may on the other hand mask true changes in membrane area. The finite kinetics of voltage-dependent currents lead to additional, more complicated effects. The approximate size of these kinetic effects in the capacitance trace may be estimated, provided that the kinetics and voltage dependence of the channels are known. Capacitance changes within the range of these effects must thus be treated with extreme caution.

In a depolarization experiment in which all currents except calcium currents and leak currents are blocked, the effects of the calcium currents on the capacitance measurement must be accounted for. Only when the kinetic parameters of the channels in the membrane potential range of the sine wave are well characterized, the artifact in the capacitance measurement may be estimated from the measured current and conductance traces, and the true time course of capacitance reflecting exocytosis and endocytosis during depolarization may be recovered.

This work has been partially supported by the Deutsche Forschungsgemeinschaft (Sfb 352, TP C5). We are indebted to Jens Coorsen and Erwin Neher for comments and discussions.

REFERENCES

Augustine, G. J., and E. Neher. 1992. Calcium requirements for secretion in bovine chromaffin cells. *J. Physiol. (Lond.).* 450:247–271.

Bielefeldt, K., J. L. Rotter, and M. B. Jackson. 1992. Three potassium channels in rat posterior pituitary nerve terminals. *J. Physiol. (Lond.)* 458:41–67.

Breckenridge, L. J., and W. Almers. 1987. Currents through the fusion pore that forms during exocytosis of a secretory vesicle. *Nature.* 328: 814–817.

Clausen, C., and J. M. Fernandez. 1981. A low-cost method for rapid transfer function measurements with direct application to biological impedance analysis. *Pflügers Arch. Eur. J. Physiol.* 390: 290–295.

Cole, K. S. 1972. Membranes, Ions, and Impulses. University of California Press, Berkeley.

Donelly, D. F. 1994. A novel method for rapid measurement of membrane resistance, capacitance, and access resistance. *Biophys. J.* 66:873–877.

Fenwick, E. M., A. Marty, and E. Neher. 1982. Sodium and calcium channels in bovine chromaffin cells. *J. Physiol. (Lond.).* 331:599–635.

Fidler, N., and J. M. Fernandez. 1989. Phase tracking: an improved phase detection technique for cell membrane capacitance measurements. *Biophys. J.* 56:1153–1162.

Gillis, K. D. 1995. Techniques for membrane capacitance measurements. *In* Single-Channel Recording, 2nd ed. B. Sakmann and E. Neher, editors. Plenum Press, New York. 155–198.

Hartmann, J., and M. Lindau. 1995. A novel Ca^{2+}-dependent step in exocytosis subsequent to vesicle fusion. *FEBS Lett.* 363:217–220.

Heinemann, C., R. H. Chow, E. Neher, and R. S. Zucker. 1994. Kinetics of the secretory response in bovine chromaffin cells following flash photolysis of caged Ca^{2+}. *Biochem. J.* 67:2546–2557.

Hodgkin, A. L., and A. F. Huxley. 1952. A quantitative description of membrane current and its application to conduction and excitation in nerve. *J. Physiol. (Lond.).* 117:500–544.

Joshi, C., and J. M. Fernandez. 1988. Capacitance measurements: an analysis of the phase detector technique used to study exocytosis and endocytosis. *Biophys. J.* 53:885–892.

Kilic, G., and M. Lindau. 1995. Calcium-activated K channels in pituitary nerve terminals as a probe for membrane calcium. *Biophys. J.* 68:396*a*. (Abstr.)

Lemos, J. R., and M. C. Nowycky. 1989. Two types of calcium channels coexist in peptide-releasing vertebrate nerve terminals. *Neuron.* 2:1419–1426.

Lindau, M. 1991. Time-resolved capacitance measurements: monitoring exocytosis in single cells. *Q. Rev. Biophys.* 24:75–101.

Lindau, M., and E. Neher. 1988. Patch-clamp techniques for time-resolved capacitance measurements in single cells. *Pflügers Arch. Eur. J. Physiol.* 411:137–146.

Lindau, M., E. L. Stuenkel, and J. J. Nordmann. 1992. Depolarization, intracellular calcium and exocytosis in single vertebrate nerve endings. *Biophys. J.* 61:19–30.

Marty, A., and E. Neher. 1985. Potassium channels in cultured bovine adrenal chromaffin cells. *J. Physiol. (Lond.).* 367:117–141.

Moore, L. E., and B. N. Christensen. 1985. White noise analysis of cable properties of neuroblastoma cells and lamprey central neurons. *J. Neurophysiol.* 53:636–651.

Neher, E., and A. Marty. 1982. Discrete changes of cell membrane capacitance observed under conditions of enhanced secretion in bovine adrenal chromaffin cells. *Proc. Natl. Acad. Sci. USA.* 79:6712–6716.

Neher, E., and R. S. Zucker. 1993. Multiple calcium-dependent processes related to secretion in bovine chromaffin cells. *Neuron.* 10:21–30.

Press, W. H., B. P. Flannery, S. A. Teukolsky, and W. T. Vetterling. 1989. Numerical recipes in pascal: the art of scientific computing. Cambridge University Press, Cambridge.

Rohlicek, V., and J. Rohlicek. 1993. Measurement of membrane capacitance and resistance of single cells with two frequencies. *Physiol. Res.* 42:423–428.

Rohlicek, V., and A. Schmid. 1994. Dual-frequency method for synchronous measurement of cell capacitance, membrane conductance and access-resistance on single cells. *Pflügers Arch. Eur. J. Physiol.* 428:30–38.

Spruce, A. E., L. J. Breckenridge, A. K. Lee, and W. Almers. 1990. Properties of the fusion pore that forms during exocytosis of a mast cell secretory vesicle. *Neuron.* 4:643–654.

Stuenkel, E. L. 1994. Regulation of intracellular calcium and calcium buffering properties of rat isolated neurohypophysial nerve terminals. *J. Physiol. (Lond.).* 481:251–271.

Tatham, P. E. R., and M. Lindau. 1990. ATP-induced pore formation in the plasma membrane of rat peritoneal mast cells. *J. Gen. Physiol.* 95:459–475.

Thomas, P., J. G. Wong, and W. Almers. 1993a. Millisecond studies of secretion in single rat pituitary cells stimulated by flash photolysis of caged Ca^{2+}. *EMBO J.* 12:303–306.

Thomas, P., J. G. Wong, A. K. Lee, and W. Almers. 1993b. A low affinity Ca^{2+} receptor controls the final steps in peptide secretion from pituitary melanotrophs. *Neuron.* 11:93–104.

Thorn, P. J., X. Wang, and J. R. Lemos. 1991. A fast transient K^+ current in neurohypophysial nerve terminals of the rat. *J. Physiol. (Lond.)* 432:313–326.

Wang, G., P. Thorn, and J. R. Lemos. 1992a. A novel large-conductance Ca^{2+}-activated potassium channel and current in nerve terminals of the rat neurohypophysis. *J. Physiol. (Lond.).* 457:47–74.

Wang, X., S. N. Treistman, and J. R. Lemos. 1992b. Two types of high-threshold calcium currents inhibited by ω-conotoxin in nerve terminals of the rat neurohypophysis. *J. Physiol. (Lond).* 445:181–199.

Yawo, H. 1990. Voltage-activated calcium curents in presynaptic nerve terminals of the chicken ciliary ganglion. *J. Physiol. (Lond.).* 428: 199–213.